

# Computational Thermal Fluid Models for Design of a Modern Fiber Draw Process

Kok-Meng Lee, *Fellow, IEEE*, Zhiyong Wei, Zhi Zhou, and Siu-Ping Hong

**Abstract**—Many manufacturing processes require time-consuming setups before automation can begin. This paper investigates the applications of distributed-parameter computational thermal-fluid models for automating the design of a continuous manufacturing system, which aims at reducing process setup time. A generic draw process is used as an example throughout this paper, which involves practically all modes of heat transfer. Two physically accurate distributed-parameter models (semi-two-dimensional (2-D) and quasi-one-dimensional (1-D)) are derived and experimentally validated. In deriving these models, we relax a number of assumptions commonly made in modeling draw processes, and extend the models to allow for 2-D static/dynamic response predictions. The semi-2-D model provides a means to accurately predict the free surface geometry and the location at which the glass solidifies into a fiber, which also serves as a basis to derive the quasi-1-D model. The quasi-1-D model that explicitly solves for the controlled variables is attractive for control system design and implementation. These results are particularly important in the optical-fiber industry because the difficulties in making precise in situ measurements in the harsh environment of the draw process have posed a significant challenge in the control of fiber diameter uniformity. Additionally, these numerically computed and experimentally measured neck-down profiles obtained in an industry setting can be used as benchmark data for future comparisons. The modeling approaches presented here are applicable to a variety of thermal-fluid systems, such as thermal processing of semiconductor wafer and food. Despite the emphasis in this paper on the faster draw of large-diameter glass that is a participating media in radiation, the technique for predicting the 2-D temperature distribution and the streamlines describing the fluid flow is equally applicable to processes involving nonparticipating media, such as composite, polymer, or synthetic fibers.

**Note to Practitioners**—This paper is motivated by a problem in the fiber draw industry because of the progressive difficulty in maintaining the diameter uniformity resulting from the ever-increasing preform (or glass rod) diameter and draw speed. The larger diameter a preform is, the longer the fiber can be drawn in the furnace from a single preform and in much less time by drawing at a higher speed. The number of setups to initiate the draw can thus be drastically lowered. The tradeoff, however, is that the glass takes a longer distance to cool into a fiber after leaving the furnace, for which an insulated post-chamber is added to gradually cool the fiber to solidification in order to reduce

optical losses in the final product. Existing models assuming a Dirichlet boundary condition at the furnace exit are valid only for drawing a small-diameter preform as long as the fiber solidifies inside the furnace. As larger preforms are drawn at higher speeds, it is necessary to locate the solidification for optimizing the post-chamber design, and to develop high-fidelity models for controlling the diameter uniformity. This paper formulates a general 2-D thermal-fluid dynamic model (which does not rely on assumptions commonly made for small preforms) to characterize the free-surface flow of the glass in both the furnace and the post-chamber. We demonstrated how a detailed description of the free surface geometry, temperature fields, and streamlines can be accurately computed from the 2-D model for process design, which also provides a basis to derive a distributed quasi-1-D model explicitly solving for the essential process state variables. Both models have been experimentally validated (with a 9-cm-diameter glass preform) by comparing against the data obtained (at 25 m/s) in an industry setting. These models have been successfully applied to the design of commercial draw towers.

**Index Terms**—Computational fluid dynamics, distributed-parameter dynamic model, draw process, numerical heat transfer, optical fibers.

## I. INTRODUCTION

**T**HERMAL-FLUID transports play an important role in the quality of final products and the design of their manufacturing processes/systems. In many automation processes, such as continuous drawing of optic fibers, direct measurement of the temperature/velocity fields and other critical distributed variables is often impossible. The current design of these processes has been relied on extensive trials-and-errors. The ability to predict the distributed variables offers an effective means to analyze the underlying physical characteristics, explain experimental observations, and optimize process designs. This paper presents two thermal-fluid models and their simulation methods for design/control of a modern draw tower capable of drawing fibers from large preforms at high speeds.

Optical fibers are manufactured from circular fused-silica glass rods (or preforms) in a draw tower shown in Fig. 1, which typically includes three sequential sections. In the preform heating section, the preform is heated above the glass melting temperature in the cylindrical furnace while it is steadily drawn into a fiber at a specified draw speed by a high tension force. The fiber is then cooled down to the ambient temperature before reaching the pressurized coating section, where the fiber is coated with an organic material and cured in the ultraviolet (UV) ovens. Finally, the coated fiber is wound on spools through a precision winding mechanism located at the base of the tower.

Manuscript received May 28, 2004; revised September 6, 2004 and March 10, 2005. This paper was recommended for publication by Editor P. Ferreira upon evaluation of the reviewers' comments. This work was supported in part by Lucent/OFS.

K.-M. Lee is with the Woodruff School of Mechanical Engineering, Georgia Institute of Technology, Atlanta, GA 30332-0405 USA (e-mail: kok-meng.lee@me.gatech.edu).

Z. Wei is with the New Technologies and Engine Component Program, Caterpillar Inc., Mossville, IL 61522 USA (e-mail: Wei\_Zhiyong@cat.com).

Z. Zhou is with the Center of Excellence for Control, Plugpower, Inc., Latham, NY 12110 (e-mail: zhi\_zhou@plugpower.com).

S.-P. Hong is with Optical Fiber Solutions, Norcross, GA 30071 USA.  
Digital Object Identifier 10.1109/TASE.2005.859657

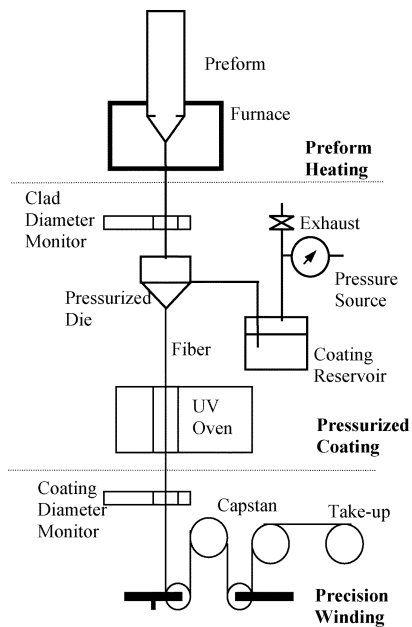


Fig. 1. Schematics showing a typical draw tower.

A typical draw cycle begins with setting up a preform in the feeding mechanism. This initial setup is often time-consuming as the preform must be fed slowly into the furnace to avoid thermal cracks [1]. Although this problem can be formulated as a robotic pick-and-place problem to replace manual setups of the preforms, a more effective way to improve productivity is to use large-diameter preforms for a given tower; thereby reducing the number of initial setups to a minimum. As an example, an increase in preform diameter from 1 to 10 cm implies that the length of a 125- $\mu\text{m}$ -diameter fiber (that can be drawn from 1-m-long preform) would be increased from 6.4 to 640 km. Furthermore, an increase in draw speed from 3 to 30 m/s would reduce the cycle time for drawing the 640-km-long fiber from 60 to 6 h. Motivated by the interest to improve productivity and reduce cost, the trend has been to use larger diameter preforms drawn at higher speeds. The tradeoff is that the glass takes a much longer distance to cool into a fiber after leaving the furnace. On the other hand, it is necessary to cool the glass gradually to solidification to reduce optical losses in the final product. Hence, an insulated post-chamber (with a small orifice through which the fiber passes) is added in most modern draw towers immediately after the furnace as shown in Fig. 2. Exceptionally stringent production requirements, along with the difficulties in making precise measurements in the furnace, have posed a significant challenge in the design/control of a modern draw process. The problem becomes one of multivariable-distributed temperature/ free-surface flow control.

The research effort investigating the effect of increasing the draw ratio (the ratio of fiber draw speed to preform feed rate) can be found in a lot of literature since the late 1960s. Most of the early studies were for textile and synthetic fibers; for example, [2]–[4]. These early studies modeled the draw process as an isothermal system and suggested that the open-loop system would become unstable when the draw ratio exceeds some critical value. Mulpur and Thompson [5] applied the isothermal

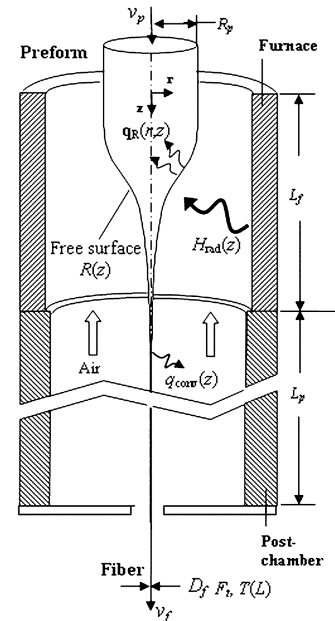


Fig. 2. Schematics illustrating the draw process.

model to design a nonlinear controller for suppressing diameter variations in optical-fiber drawing processes. Arguing that the open-loop system would become unstable when the logarithmic draw ratio exceeds a critical value of 3.15, their control objective was to stabilize the draw process. In contrast to these results, Pearson *et al.* [6] and Mhaskar and Shah [7] showed that the process is unconditionally stable when the (Newtonian) fluid freezes into a fiber before reaching the windup spool. Their models were, however, highly simplified and generally neglected one or more terms among the advection, the radiative transfer, and conduction. In a later study that was based on the conservation of energy, Geyling and Homsy [8] showed that the process stability depended not only on the draw ratio, but also on convective and radiative heat transfer. During the same period, rigorous thermal-fluid models for drawing optical fibers were developed. Early studies primarily focused on one-dimensional (1-D) models for drawing fibers from small-diameter preforms at a relatively slow speed (for example, [9]–[12]).

To develop a more accurate two-dimensional (2-D) model for optimizing the draw process, Xiao and Kaminski [13] solved the 2-D conjugate problem of the glass and gas flow with free interface using commercial finite-element code FIDAP. Their results (computed for a 5-cm-diameter preform) showed that while the glass temperature has 2-D distribution, the glass velocity distribution could be approximated as 1-D. They also reported difficulties to ensure convergence (that is sensitive to the deformation mesh) as the number of radiative macro surfaces increases. Choudhury *et al.* [14] used a 1-D axial velocity and force balance equations to compute the neck-down profile while solving for the temperature using the 2-D heat transfer and fluid flow. Small-diameter (1.25-cm) preforms drawn at 3 m/s was considered in their simulations.

More recently, Yin and Jaluria [15] and Cheng and Jaluria [16] investigated the effects of some parameters on high-speed fiber drawing (up to 20 m/s). As most of the previous studies,

they assumed that the glass was drawn into the specified fiber diameter of 125  $\mu\text{m}$  before leaving the furnace exit. Their results, however, show that the computed glass temperatures were well above the glass melting point at the furnace exit, indicating that the glass is still converging after leaving the furnace and that the actual diameter (and, hence, the speed) of the glass at the furnace exit is essentially unknown. Previous studies [17] suggest that models assuming a Dirichlet boundary condition at the furnace exit are valid only for drawing a small-diameter preform as long as the glass fiber solidifies within the furnace. As larger preforms are drawn at higher speeds, it is necessary to determine the location at which the glass converges into a fiber in optimizing the post-chamber.

Another factor that significantly influences the draw efficiency is the radiation between the furnace and the participating glass; a dominant mode of heat transfer in the draw process. Homsy and Walker [10] found that the Rosseland diffusion approximation, which is an assumption commonly used in many early studies in solving the radiative transfer in the semitransparent glass, would fail at the surface. This finding was confirmed in a similar study [1], where the radiative transfer equation (RTE) was numerically solved using discrete ordinate method (DOM) to predict the temperature gradient built up during transient. The analysis in [1] further showed that the glass absorption coefficient in the short-wavelength band cannot be neglected and proposed a modified band model that includes the glass absorption at short wavelengths. Another approach, the finite volume method (FVM), has been investigated for modeling semitransparent, emitting, and absorbing medium. The FVM has a flexibility to lay out the spatial and angular grids. Liu *et al.* [18] compared the FVM and DOM on a benchmark problem, which show reasonably good agreements and, in some cases, the FVM outperformed the DOM.

In order to provide a rational basis for deriving an accurate dynamic model explicitly solving for the controlled variables of an automated draw process basis and for automating the design of a modern draw tower, we offer the following in this paper.

- 1) Two thermal-fluid dynamic models, which relax several assumptions commonly made for small preforms, were developed to characterize the complete neck-down shape at steady-state and during the transient. These models incorporating practically all modes of heat transfer will provide a basis for automating the design process of a modern fiber draw. Yet, the models and the draw system are generic and applicable to a broad spectrum of thermal-fluid systems.
- 2) Both models have been experimentally validated and successfully applied to the design of commercial draw towers. Unlike previous studies where experimental data were obtained for a small-diameter preform (1.25 cm) and at low speed (3 m/s), we verify our prediction against an experimentally measured neck-down profile for a 9-cm-diameter preform drawn at 25 m/s. The success in drawing fibers from larger preforms at high speeds results in a significant reduction in overall setup time; thereby greatly improving productivity and reducing labor cost—a common interest in many industries (for example, rapid thermal processing systems in the semiconductor industry [19]).
- 3) Through a practical fiber draw application, we demonstrate how these models can be used to analyze the flow of loose particles from the walls of the furnace/post-chamber, which could stick on the melting glass and break the moving fiber. This is particularly important from the automation standpoint since a manual reset-up (due to any breakage of the moving fiber) will increase production cost.
- 4) The models provide a means to uniquely determine the length of the post-chamber, which is critical to optimize the draw system design. The studies were validated by comparing two methods of locating the fiber solidification and by comparing the computed temperatures at the inner wall and at the exit of the post-chamber against those measured experimentally.

## II. GOVERNING EQUATIONS

We consider the thermal fluid transports in a generic draw system consisting of a furnace and a post-chamber as shown in Fig. 2. The glass is drawn from a preform (with a diameter of several centimeters) into a fiber (for example, 125- $\mu\text{m}$  diameter). Since the viscosity of the fused silica is an exponential function of temperature [20], the viscous flow is strongly coupled with the thermal transport within the glass.

The highly viscous-free surface flow forms a neck-down profile in the furnace, which is dominantly heated by means of radiation emission from the high-temperature furnace wall. The radiation heat flux is partly adsorbed and reflected at the glass surface while a majority of it is transferred through the semitransparent glass media. Some of the challenges in computing the radiative transfer are the following: 1) the radiation intensity depends not only on wavelength but also on the location/orientation variables; 2) the boundary condition at the glass-free surface is complicated since the surface irradiations cannot be directly obtained; 3) the view factor is difficult to calculate due to the arbitrary geometry.

The converging glass is cooled by a mixed convection of air involving the boundary layer flow around continuously moving fiber and the natural convection in the open-ended chamber. The difficulties in computing the mixed convection is as follows: 1) most of the boundary layer flow in the post-chamber is around a high-speed moving glass with a diameter of much less than 1 mm; 2) the buoyancy force and the drag force are in the opposite direction; sharp temperature and velocity gradients exist within the boundary layer. In the following discussion, we consider two general approaches in formulating the furnace/post-chamber system.

### A. 2-D Formulation

The general 2-D governing equations for the conservation of mass, momentum, and energy in cylindrical coordinate system are given by (1), (2), (3), and (4), respectively, [21]

$$\frac{\partial \rho}{\partial t} + \frac{1}{r} \frac{\partial}{\partial r} (r \rho u) + \frac{\partial}{\partial z} (\rho v) = 0 \quad (1)$$

$$\rho \frac{Du}{Dt} = \frac{1}{r} \frac{\partial(r\sigma_{rr})}{\partial r} + \frac{\partial\sigma_{rz}}{\partial z} - 2\mu \frac{u}{r^2} \quad (2)$$

$$\rho \frac{Dv}{Dt} = \frac{1}{r} \frac{\partial(r\sigma_{rz})}{\partial r} + \frac{\partial\sigma_{zz}}{\partial z} + \rho g \quad (3)$$

$$\rho C_p \frac{DT}{Dt} = \frac{1}{r} \frac{\partial}{\partial r} \left( k_m r \frac{\partial T}{\partial r} \right) + \frac{\partial}{\partial z} \left( k_m \frac{\partial T}{\partial z} \right) + W_i + \mu \Phi \quad (4)$$

where

$$\begin{aligned} \frac{D}{Dt} &= \frac{\partial}{\partial t} + u \frac{\partial}{\partial r} + v \frac{\partial}{\partial z} \\ \sigma_{rr} &= -p + 2\mu \frac{\partial u}{\partial r} \\ \sigma_{rz} &= \mu \left( \frac{\partial u}{\partial z} + \frac{\partial v}{\partial r} \right) \\ \sigma_{zz} &= -p + 2\mu \frac{\partial v}{\partial z} \\ \Phi &= 2 \left[ \left( \frac{\partial u}{\partial r} \right)^2 + \left( \frac{u}{r} \right)^2 + \left( \frac{\partial v}{\partial z} \right)^2 \right] + \left( \frac{\partial u}{\partial z} + \frac{\partial v}{\partial r} \right)^2 \end{aligned}$$

and where the dependent variables  $p$ ,  $u$ ,  $v$ , and  $T$  are the pressure, the radial, and axial components of velocity and the temperature, respectively;  $\rho$ ,  $\mu$ ,  $k_m$ , and  $C_p$  are the density, viscosity, thermal conductivity, and specific heat of the fluid being considered respectively;  $g$  is the gravitational acceleration; and  $W_i$  is the heat generation per-unit volume and time. The free-surface geometry is a function of  $z$  and must be solved implicitly along with the solution to (1)–(4) for the four unknowns ( $p$ ,  $u$ ,  $v$ , and  $T$ ), which depends on the boundary conditions imposed on the system being studied.

### B. Incompressible 1-D Formulation

In the interest to provide a simple yet practical formulation for deriving a more tractable model, we consider a 1-D approximation for characterizing the free-surface flow of the glass with the following assumptions.

- 1) The velocity and temperature variations in the radial direction are neglected.
- 2) The surface tension and the air-side normal stress are considered very small.
- 3) The total axial stress can be expressed using the elongation model [9]  $\sigma_{zz} = 3\mu(\partial v/\partial z)$ .

The 1-D model can be derived by considering a differential control volume (or a disk with a circular cross-sectional area “ $a$ ” and length “ $\Delta z$ ”) as follows. Using truncated Taylor series expansion and neglecting higher order terms, the net rates of mass, axial momentum, and energy flow out through the control surface are given, respectively, by  $\frac{\partial}{\partial t}(\rho a \Delta z)$ ,  $\frac{\partial}{\partial t}(\rho a v \Delta z)$ , and  $\frac{\partial}{\partial t} \left[ \rho a \Delta z \left( e + \frac{v^2}{2} \right) \right]$ , where  $e$  and  $v^2/2$  are the thermal internal and kinetic energies, respectively. For incompressible flow ( $\partial \rho / \partial t = 0$ ), the 1-D continuity equation is given by (5)

$$\frac{\partial a}{\partial t} + \frac{\partial}{\partial z}(av) = 0 \quad (5)$$

where  $a(z, t)$  is the glass cross-sectional area of radius  $R(z, t)$  and  $v(z, t)$  is the axial velocity of the glass flow. The 1-D momentum equation can be derived by noting that two kinds of forces acting on the differential body  $a\Delta z$  are the gravitational force and the viscous normal stress

$$\frac{\partial}{\partial z}(a\sigma_z)\Delta z + \rho g a \Delta z.$$

Using Newton’s 2nd law and the elongation model, the 1-D momentum equation is reduced to (6)

$$\rho \left[ \frac{\partial(av)}{\partial t} + \frac{\partial(av^2)}{\partial z} \right] = \frac{\partial}{\partial z} \left[ 3a\mu \frac{\partial v}{\partial z} \right] + \rho g a. \quad (6)$$

The energy leaving the control volume involves flow due to the conduction across the top/bottom surfaces of the disk, the convection, and radiation across the circumferential area of the disk, and the work done on the disk by viscous stresses, which are, respectively, given by  $\frac{\partial}{\partial z} \left( k a \frac{\partial T}{\partial z} \right) \Delta z$ ,  $2\pi R(q_r'' + q_c'')$ , and  $\frac{\partial}{\partial z} [(a\sigma_z)v] \Delta z$ . Thus, the conservation of energy for the 1-D model is given by

$$\rho C_p \left[ \frac{\partial(aT)}{\partial t} + \frac{\partial(avT)}{\partial z} \right] = \frac{\partial}{\partial z} \left[ a k_{\text{eq}} \frac{\partial T}{\partial z} \right] - 2\pi R(q_r'' + q_c'') + 3a\mu \left( \frac{\partial v}{\partial z} \right)^2 \quad (7)$$

where  $q_r'' = \tilde{\epsilon}(\tilde{E} - \tilde{H})$ ;  $q_c'' = h(T - T_a)$ ;  $k_{\text{eq}} = k_m + \tilde{k}$   $T(z, t)$  is the glass temperature;  $\tilde{k}(T)$  is the apparent Rosseland’s conductivity that accounts for the radiative transfer in the participating medium such as glass;  $\tilde{\epsilon}$  is the apparent emissivity;  $\tilde{E}(T)$  is the total emissive power given by  $\sigma T^4$ ;  $\tilde{H}(T)$  is the apparent irradiation from the furnace;  $h$  is the convective heat-transfer coefficient; and  $T_a$  is the radially lumped air temperature.

Unlike the 2-D formulation where the surface profile is solved implicitly, the quasi-1-D formulation explicitly solves for the glass geometry, velocity, and temperature. Equations (5)–(7) also involve a smaller set of boundary conditions. However, the solution to the 1-D energy equation requires a good understanding of the parameters involved; namely,  $\tilde{k}$ ,  $\tilde{H}$ , and  $h$ , which are temperature dependent. Thus, we solve the complete 2-D model for the steady-state (radiative and convective) heat fluxes at the free surface so that the parameters for the 1-D model (about an operating condition) can be determined. The 2-D solution will provide significant insights to the velocity and temperature fields. Equations (5)–(7) are referred as a quasi-1-D model since the parameters ( $\tilde{k}$ ,  $\tilde{H}$ ,  $T_a$ , and  $h$ ) are derived from the steady-state solution of the 2-D model.

### III. COMPUTATIONAL MODELS

The furnace/post-chamber system can be separated into two domains, namely, the glass and air domains. Equations (1)–(4) are valid for both the glass and air domains. In the glass domain,  $W_i = -\nabla \cdot \mathbf{q}_R$  where  $\mathbf{q}_R$  is the radiative heat flux in the participating glass media. Since air is a nonparticipating medium and has very small viscosity, the heat generation term  $W_i$  and the viscous dissipation term  $\mu \Phi$  in (4) are set to zero in the air domain.

### A. Radiative Transfer

The energy equation in the glass domain requires the divergence of the radiation heat flux [22]

$$\nabla \cdot \mathbf{q}_R = \int_0^\infty \left[ 4\pi\kappa_\lambda n_\lambda^2 I_{b\lambda}(T) - k_\lambda \int_{\Omega=4\pi} I_\lambda(\mathbf{r}, \mathbf{s}) d\Omega \right] d\lambda \quad (8)$$

where the spectral radiative intensity  $I_\lambda(\mathbf{r}, \mathbf{s})$  is a function of the position vector  $\mathbf{r}$ , orientation vector  $\mathbf{s}$ , and wavelength  $\lambda$ ;  $I_{b\lambda}(T)$  is the spectral intensity of a blackbody radiation given by the Planck's function;  $\kappa_\lambda$  is the spectral absorption coefficient; and  $n_\lambda$  is the spectral index of refraction.

The radiative intensity can be obtained by solving the radiative transfer equation (RTE) [22]

$$\mathbf{s} \cdot \nabla I_\lambda(\mathbf{r}, \mathbf{s}) = \kappa_\lambda [n_\lambda^2 I_{b\lambda}(T) - I_\lambda(\mathbf{r}, \mathbf{s})]. \quad (9)$$

The RTE can be solved using a number of methods; for example, DOM or FVM for the radiation intensities. The detail of the FVM, along with the boundary conditions at the bounding interfaces of the glass media, can be found in our earlier paper [17]. Once  $I(\mathbf{r}, \mathbf{s})$  is solved, the divergence of the radiation heat flux is calculated from the integral (8).

### B. Air Domain

The boundary conditions for (1)–(4) in the air domain are detailed as follows. Along the nonslip free surface and the furnace/post-chamber walls, we have

$$r = R(z) \quad u = u_g \quad v = v_g \quad T = T_g \quad (10)$$

$$r = R_{\text{fur}} \quad u = v = 0$$

$$T = \begin{cases} T_{\text{fur}} & 0 \leq z < L_f \\ T_{\text{post}} & L_f \leq z \leq L(L_f + L_p) \end{cases} \quad (11)$$

where  $u_g$ ,  $v_g$ , and  $T_g$  are the radial and axial velocity components and the temperature along the glass free surface, respectively;  $T_{\text{fur}}$  and  $T_{\text{post}}$  are the furnace and post-chamber temperature, respectively;  $R_{\text{fur}}$  is the furnace radius;  $L_f$  is the furnace length; and  $L_p$  is the post-chamber length.

At the top of the furnace, the buoyancy driven open-ended channel air flows out of the furnace to the ambient. We extrapolate the velocity and temperature from the interior values since the downstream has negligible effects on the upstream

$$z = 0 \quad \frac{\partial u}{\partial z} = \frac{\partial v}{\partial z} = \frac{\partial T}{\partial z} = 0, \quad p = p_\infty. \quad (12)$$

At the post-chamber exit, the fiber is drawn through a small orifice (radius  $R_o$ ) through which the convective air flow is controlled by an iris. Thus, the post-chamber exit consists of an iris and an orifice in the computation domain: Around the iris where  $z = L$  and  $r > R_o$ , nonslip boundary conditions are imposed. In the orifice between the fiber and iris, the velocity components are extrapolated from the interior values. The air temperature is prescribed based on the direction of the air flow. When the air flows into the chamber, its temperature is equal to the ambient value. For the air inside the boundary layer around the moving fiber, the air temperature is extrapolated from the interior value.

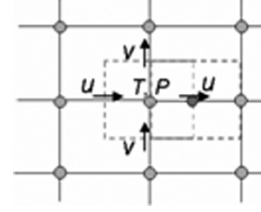


Fig. 3. Staggered grids.

The pressure is determined from the Bernoulli equation along a streamline. Thus, at  $z = L$

$$r > R_o \quad u = v = 0, \quad T = T_{\text{iris}}$$

$$p - p_\infty = -\frac{\rho \bar{v}^2}{2} \quad \frac{\partial u}{\partial z} = \frac{\partial v}{\partial z} = 0 \quad (13)$$

$$r < R_o \quad \begin{cases} \frac{\partial T}{\partial z} = 0 & (v > 0) \\ T = T_{\text{amb}} & (v < 0) \end{cases} \quad (14)$$

where  $T_{\text{iris}}$  is the iris temperature and

$$\bar{v} = \frac{2}{R_o^2 - R_f^2} \int_{R_f}^{R_o} vr dr. \quad (15)$$

In the air domain, we extend the application of the pressure-implicit with splitting of operators (PISO) numerical algorithm [23] to solve (1)–(4), along with the boundary conditions (10)–(25) in curvilinear coordinates with staggered grids. The staggered grids (as illustrated in Fig. 3) are used in solving the flow equations. In the staggered grid system, the temperature, pressure, and all of the physical properties are defined at the center node of each cell, while velocity components  $u$  and  $v$  are defined at the cell faces, whose control volumes are half a grid staggered from those of  $p$  and  $T$  as shown in Fig. 3. This scheme avoids the need for an explicit boundary condition for the pressure at the free surface and fluctuations in the solution (due to the central differencing of the first derivative terms) at the free surface.

### C. Glass Domain (Incompressible Semi-2-D Formulation)

Draw processes often involve incompressible highly viscous fluid flow, where velocity variations in the radial direction are greatly reduced by the strong shear stresses. As a result, the velocity distribution is almost 1-D. The computation in the glass domain can be significantly simplified by using a semi-2-D formulation, which solves for the 2-D temperature field and 1-D velocity profile from (4)–(6). The radial velocity component in the 2-D energy equation (4) is obtained by integrating (1) with respect to  $r$  so that the 2-D continuity equation is satisfied

$$u(r, z) = -\frac{r}{2} \frac{dv}{dz}. \quad (16)$$

For fiber diameter control, both the furnace and post-chamber must be included in the computation since the glass may not solidify before leaving the furnace; the axial velocity of the glass at the furnace exit is essentially unknown. In order to reduce optical loss, the fiber must solidify with a relatively slow cooling rate into a constant diameter within the post-chamber.

The boundary conditions for the semi-2-D model are as follows. The glass is axisymmetric and, thus, along the centerline

$$\text{At } r = 0 \quad \frac{\partial T}{\partial r} = 0. \quad (17)$$

At the furnace inlet, the preform (of radius  $R_p$ ) enters with a uniform feedrate  $v_p$  and loses heat to its surroundings through convection. Due to the presence of the conduction heat transfer, the glass temperature may not reach a developed condition. To reduce the computation time, we linearly extrapolate the temperature from the interior of the furnace in the numerical solution to the problem since no significant temperature differences were found in the simulations when more detailed temperature boundary conditions were considered. We thus specify a zero diffusion condition at the furnace inlet

$$z = 0 \quad R = R_p \quad u = 0 \quad v = v_p \quad \frac{\partial^2 T}{\partial z^2} = 0. \quad (18)$$

At the exit of the post-chamber, the fiber velocity is equal to the draw speed  $v_f$ . The fiber temperature, however, may not have fully developed due to the viscous dissipation and, thus, we prescribe a zero diffusion condition to extrapolate the fiber temperature from the interior as the temperature outside the domain does not have considerable effects on the upstream temperature of the glass at

$$z = L \quad \frac{du}{dz} = 0 \quad v = v_f \quad \frac{\partial^2 T}{\partial z^2} = 0. \quad (19)$$

The 1-D velocity approximation reduces the steady-state velocity to a simple form. From the mass conservation, we have the following relationship:

$$v = \frac{v_p R_p^2}{R^2}. \quad (20)$$

We substitute the above equation into the steady-state form of (6), which is followed by integrating the resulting equation twice with respect to  $z$ . Upon substituting the boundary conditions for  $v(0) = v_p$  and  $v(L) = v_f$ , we obtain the following expression for  $v(z)$ :

$$v(z) = v_p - \int_0^z \left( \frac{\rho g \int_0^z R^2 dz + 2\rho R_p^4 v_p^2 \int_0^z \frac{dr}{r^3} - C_1}{3\mu R^2} \right) dz. \quad (21)$$

where

$$C_1 = \frac{v_f - v_p + \frac{\rho}{3} \int_0^L \frac{1}{\mu R^2} \left[ g \int_0^z R^2 dz + \frac{R_p^2 v_p^2}{\mu R^2} \left( 1 - \frac{R_p^2}{R^2} \right) \right] dz}{\int_0^L \frac{1}{\mu R^2} dz}.$$

Once the axial velocity  $v(z)$  is obtained, the free surface profile of the glass can be obtained from

$$R(z) = R_p \sqrt{\frac{v_p}{v(z)}}. \quad (22)$$

Equations (21) and (22) implicitly relates  $v(z)$  and  $R(z)$ , which must be solved iteratively. In solving for the velocity distribution, the glass viscosity  $\mu(T)$  is determined based on the radially lumped temperature

$$\bar{T}(z) = \frac{2}{R^2(z)} \int_0^{R(z)} T(r, z) dr. \quad (23)$$

#### D. Procedure for Computing the Steady-State Solution

The computation is performed in curvilinear coordinates. The method for transforming from cylindrical to curvilinear coordinates can be found in [24].

The solution to the free surface profile is challenging since it requires solving simultaneously the governing equations for the glass and air domains as well as the radiative transfer and the enclosure analysis. Multiple loops of iterations are needed to obtain the numerical solution, which makes the convergence of the computation a challenge. We develop a computation procedure based on decoupling the temperature iteration from the free surface iteration. This procedure, which effectively reduces the degree of freedoms (unknown variables) during the computation iterations and has been found to be robust and efficient, is outlined as follows.

- Step 1) Assume initial values for the surface profile  $R(z)$  and the primitive variables  $v(z)$  and  $T(r, z)$ .
- Step 2) Conjugate temperature iteration (for a given free surface and glass velocity distribution).
  - a) Calculate the  $u(z)$  from (16).
  - b) Solve the 2-D governing equations for the mixed convection problem in the air domain using the PISO algorithm [23] and then calculate the convective heat flux along the free interface  $q_{\text{conv}} = k_a (\partial T / \partial n)|_a$ .
  - c) Solve the RTE and its boundary conditions using the FVM [17]. At the same time, obtain the furnace radiosities through the enclosure analysis. Then, calculate  $W_i = -\nabla \cdot \mathbf{q}_R$  using the solved intensities.
  - d) Solve the 2-D glass energy equation using the implicit time marching scheme [24].
  - e) Repeat Step 2(c) until a steady-state solution of the glass temperature is reached.
  - f) Repeat Step 2(b) until the glass temperature does not vary between two consecutive iterations in this step.
- Step 3) Free surface and velocity field computation (for a calculated glass temperature field from Step 2).
  - a) Calculate the glass viscosity based on the radially lumped temperature defined in (23).
  - b) Calculate 1-D glass velocity  $v(z)$  using (21).
  - c) Update the free-surface profile using (22).
  - d) Repeat Step 3(b) until the free-surface profile does not change between two consecutive iterations.
- Step 4) Regenerate the 2-D curvilinear grid, and then repeat Step 2 until the relative change between two consecutive computed free-surface profiles at Step 4 is less than  $10^{-5}$ .

#### E. Procedure for Dynamic Simulation

The parameters ( $\tilde{H}$ ,  $h$ ,  $T_a$ , and  $\tilde{k}$ ) in the quasi-1-D model can be obtained once the steady-state solution of the semi-2-D is computed, upon which the reduced-order models for characterizing the perturbation dynamics of the free-surface glass flow can be developed for the design of a model-based controller [25]. The parameters in quasi-1-D are computed as follows.

The apparent irradiation is given by

$$\tilde{H} = \tilde{E} - \frac{q_r''}{\tilde{\epsilon}} \quad (24)$$

where the apparent emissivity  $\tilde{\epsilon}$  can be obtained using correlation given in [11]. The steady-state values of the above apparent variables can be obtained from the 2-D numerical solution of the radiation heat flux and the glass temperature

$$q_r'' = \int_0^\infty (J_\lambda - H_\lambda) d\lambda \quad (25)$$

where  $J_\lambda$  and  $H_\lambda$  are the radiosities and irradiation on the glass outer surface, respectively; the method for computing these quantities is given in [1].

The convective heat-transfer coefficient  $h$  can be calculated from (26)

$$h = \frac{q_c''}{T - T_a} \quad (26)$$

where the radially lumped air temperature  $T_a$  can be obtained from the 2-D solution of the air temperature field.

We model the radiative transfer in the axial direction in the form of a Rosseland conductivity

$$\tilde{k} = \frac{16n_g^2\sigma T^3}{3\tilde{\kappa}_R} \quad (27)$$

where  $n_g$  is the average index of the refraction of the glass. The apparent absorption coefficient  $\tilde{\kappa}_R$  in (27) accounts for the fact that the media is not optically thick, which can be obtained using the steady-state radiative flux and temperature field.

The procedure for computing the dynamic (transient) responses (from semi-2-D or quasi-1-D model) is as follows:

- Step 1) Specify the initial conditions.
- Step 2) Using the value at the  $i^{\text{th}}$  time step,  $a(z, t_i)$ , and  $v(z, t_i)$  to solve (5) and (6) for  $a(z, t_i + 1)$  and  $v(z, t_i + 1)$ .
- Step 3) Solve for 2-D or 1-D temperature fields as follows.  
*Semi-2-D model:* Calculate  $u(r, z, t_{i+1})$  from (16); iteratively solve (9) and (4) for  $T(r, z, t_{i+1})$  and then calculate  $\bar{T}(z, t_{i+1})$ .  
*Quasi-1-D model:* Solve (7) for  $T(z, t_{i+1})$ .
- Step 4) Update the viscosity  $\mu(T)$ , then repeat Steps 2 and 3 until the relative changes of  $v$  and  $T$  between two adjacent iterations are less than  $10^{-6}$ .
- Step 5) Save the values of the variables at the current time step, forward the simulation time by  $\Delta t$ , and return to Step 2 until the end of the simulation period is reached.

#### IV. RESULTS

A MATLAB program with C++ subroutines has been written to predict the temperature/velocity fields of a modern optical-fiber drawing process. The values for the simulation as shown in Table I were data provided by OFS (Norcross, Georgia) so that models and numerical results can be validated experimentally. Thus, the temperature distribution of the furnace wall was

TABLE I  
PARAMETERS USED IN THE SIMULATION

Tower Configurations		TC-I	TC-II
Specified	fiber radius, $R_f$ ( $\mu\text{m}$ )	62.5	62.5
	draw speed, $v_f$ (m/s)	25	25
	draw tension, $F_t$ (grams)	90	110
Preform	radius, $R_p$ (m)	0.045	0.045
	peak temperature, $T_{f,max}$ (K)	2,325	2,396
Furnace	minimum temperature, $T_{f,min}$ (K)	1,928	1,848
	radius, $R_{fur}$ (m)	0.06	0.06
	length, $L_f$ (m)	0.45	0.45
Post-chamber	radius, $R_{post}$ (m)	0.06	0.06
	length, $L_p$ (m)	2.7	1.229

measured experimentally using a M90R single-color infrared thermometer (MIKRON, Inc.), which measures the radiosities at 0.65- $\mu\text{m}$  wavelength. This was followed by radiation analysis on the enclosure to obtain the emission intensities and, consequently, the temperature of the furnace wall. The furnace temperature is parabolic with the maximum at the middle and minimum at both ends.

The glass preform is made of fused silica. The absorption coefficients are given in [1]. The other physical properties are taken from [26]. Experimental correlation of glass viscosity was obtained from [20]

$$\mu(T) = 0.1 \exp\left(-14.368 + \frac{61\,939.539}{T}\right). \quad (28)$$

A nonuniform grid is used with a denser spacing near the free interface and the walls. In the air domain, the dimension of the first grid adjacent to the fiber surface should be at least less than half of the fiber radius (i.e., 30  $\mu\text{m}$ ) in order to account for the sharp gradients in the boundary layer. After a grid size study and refinement, the grid numbers of  $200 \times 15$  and  $160 \times 34$  (in  $z$  and  $r$  directions, respectively) are used in the glass and the air domain, respectively.

The steady-state solutions to the semi-2-D model are computed by using the procedure outlined in Section III-D for the free surface profile, temperature, and velocity fields, and the heat fluxes. The results are broadly divided as follows.

##### Steady-state solution (TC-I)

TC-I (that has a relatively long post-chamber length of 2.7 m) was used to compute the steady-state solution so that the effects of high draw speed on the following can be analyzed:

- 1) heat flux calculation and flow field simulation;
- 2) steady-state free-surface profile prediction;
- 3) effects of draw-speed on fiber diameter and temperature.

##### Transient response (TC-II)

TC-II (with a shorter length of 1.229 m) was used in simulating the transient responses, for which the furnace temperature and the draw tension were calibrated so that the glass converges to 125  $\mu\text{m}$ -diameter fiber at the post-chamber exit. The shorter chamber length reduces the computation burden since all numerical algorithms were implemented on a desktop PC.

Since measurement of the in situ glass temperature and velocity, radiative, and convective heat flux are extremely difficult inside the high-temperature furnace/post-chamber environment, we validated the semi-2-D and quasi-1-D steady-state solution

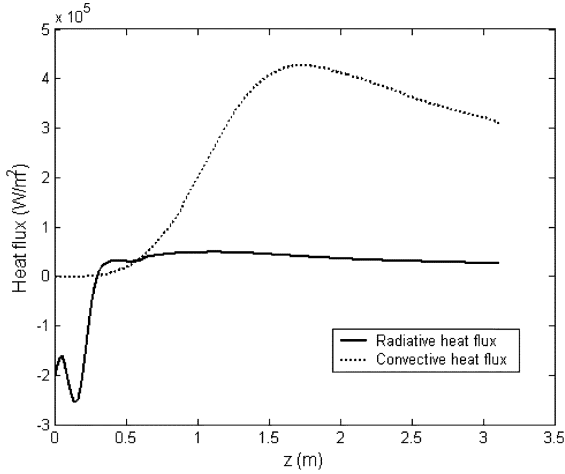


Fig. 4. Heat fluxes along the free surface.

by comparing the predicted free-surface radii against those measured experimentally. We also validate the computation of the mixed air convection model by measuring the fiber temperature at the post-chamber exit and the inner wall temperature of the post-chamber.

#### A. Heat-Flux Calculation and Flow-Field Simulation

As shown in (7), the solution to the quasi-1-D energy equation requires the knowledge of the air convective and radiation heat fluxes  $q_c''$  and  $q_r''$ , along the free surface of the glass, which have been computed and plotted in Fig. 4 using the 2-D numerical solution. The results show that in the neck-down region inside the furnace  $q_c''$  is negligible compared to  $q_r''$  as expected since the heating of the neck-down region is dominated by radiation, but  $q_c''$  becomes significant in the post-chamber where the glass is primarily cooled by air convection due to the high surface-area to volume ratio and the high moving speed of the glass. Once the 2-D solution is obtained, the parameters ( $\tilde{k}$ ,  $\tilde{H}$ ,  $h$ , and  $T_a$ ) in (7) can then be calculated.

For the automation standpoint, it is essential to prevent any loose particles from the post-chamber wall to stick on the melting glass (and break the moving fiber) since a manual reset-up the draw process will be required for any breakage of the moving fiber. The 2-D solution to (1)–(4) along with the boundary conditions given in Section III-B for the air domain provides a detailed description of the temperature and velocity fields. To help visualization and analysis for the design of mixed air convection flow in the post-chamber, we obtain streamlines from the velocity fields, which are lines everywhere tangent to the velocity fields. The stream function is obtained using the following radial integration:

$$\psi(r) = \psi(0) - \int_0^r sv(s)ds \quad (29)$$

where  $s$  is a dummy variable for the integration. For a steady-state flow, streamlines are fixed in space. Fig. 5 shows the 2-D temperature contours (lefthalf) and streamlines (righthalf) of the air inside the furnace and the post-chamber. As shown in Fig. 5, the air temperature at the furnace exit is still well above the glass melting temperature (1580 °C) and its gradient in the radial direction is very small. The glass then cools as it moves

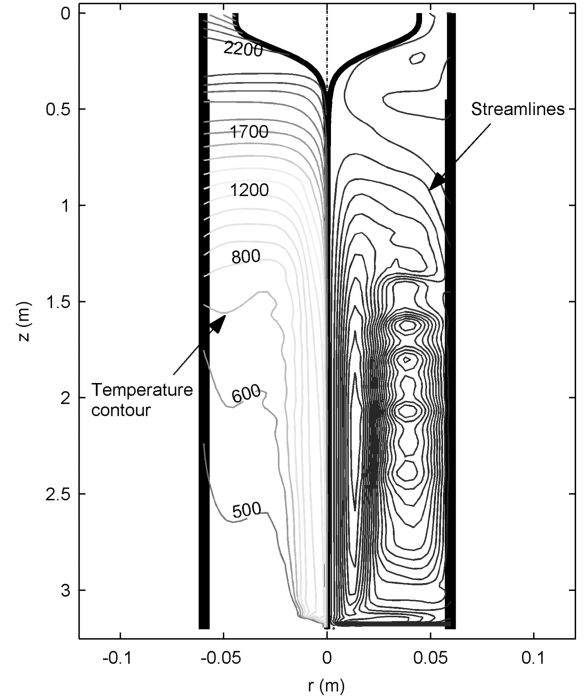


Fig. 5. Two-dimensional temperature contour and streamlines of the air.

downstream by the mixed air convection, where a boundary layer of air develops and grows downward around the continuously very-fast-moving glass (cylinder of very small cross-section) as illustrated by the streamlines on the righthalf of Fig. 5. Since the air inside the boundary layer has a higher temperature than the other region, the air close to the layer is heated and flows upward by the buoyancy force. In the local region along the post-chamber wall, air is also heated and flows upward to form a natural convection boundary layer. The air between these two upward-flowing streams flows downward to support the circulation. The circulation close to the wall is broken into several smaller rings due to the long space in the axial direction. The structure of the air flow suggests that particles leaving the post-chamber wall cannot easily reach inside the boundary layer around the moving glass.

#### B. Experimental Verification (Steady-State Solution)

We measured the steady-state-free surface profiles of the glass in the furnace domain. In the experiment, the preform was moved out of the furnace quickly (less than 1 min) in order to prevent shape deformation while the view factors were changed. After the glass cooled down, the neck-down profile was measured by a laser scanner. Since the glass in the post-chamber had a small diameter and could break easily while the space for moving the preform was limited, only the neck-down profile in the furnace domain was measured. The remainder of the glass was cut before the preform was taken out.

Fig. 6 compares the predicted free-surface profiles against the measured one at a draw speed of 25 m/s. The free-surface profiles computed using the semi-2-D and quasi-1-D models well match those measured experimentally. Some discrepancies near

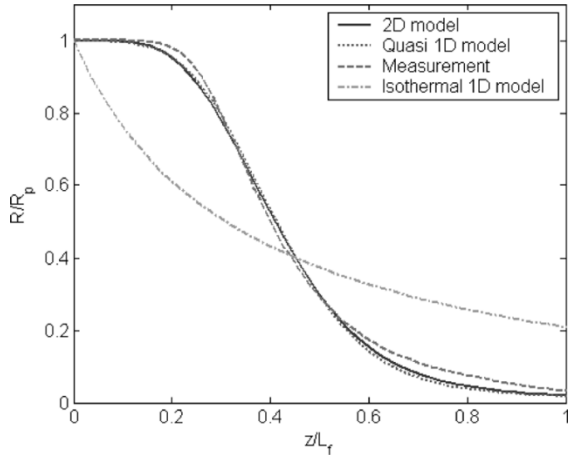


Fig. 6. Predicted and measured free-surface profiles.

the furnace exit can be explained as follows. When the pre-form is cut for removal from the furnace, the tension exerted by the draw mechanism disappears. Consequently, the velocity gradient (and, hence, the free surface slope) near the bottom of the stub decreases since it is proportional to the normal tension force as predicted by the elongation model  $\sigma_{zz} = 3 \mu dv/dz$ . Hence, the measured free-surface profile near the furnace exit has a smaller slope and larger diameter than that in the steady-state draw process, on which the predictions are based. It follows that the prediction errors near the furnace exit could be smaller than that shown in Fig. 6. Modeling errors, such as the surface radiation properties and the furnace temperature measurement errors, may also contribute to the discrepancy in the neck-down region somewhat. As shown in Fig. 6, the isothermal model, which does not consider the energy equation and, thus, assumes a constant viscosity (2000 °C), fails to predict the stable free-surface profile of the simulated process that has a logarithmic draw ratio of 5.71.

### C. Effect of Draw-Speed on Post-Chamber Design

For optimizing the design of the post-chamber, it is essential to determine the location at which the glass cools to form a solid fiber. We compare two different methods of locating the fiber solidification. The first method locates the fiber melting temperature (1580 °C) along the glass fiber. In the second method, we define the location where the glass reaches within a bound of 0.25% about the steady-state diameter of 125  $\mu\text{m}$ .

Fig. 7 shows the computed axial-temperature distributions (normalized to the glass melting point) for four different draw speeds of 18, 25, 30, and 35 m/s. Fiber solidification is rather a gradual monotonically process than those of crystalline materials with a single-phase transition temperature. The corresponding glass diameter (normalized to steady-state fiber diameter of 125  $\mu\text{m}$ ) converging to fibers in the post-chamber is graphed in Fig. 8. The two methods of locating the solidification agree reasonably well as compared in Table II. The glass viscosity at the melting temperature is very high and behaves like a solid and, hence, its melting temperature can be reasonably used to locate the fiber solidification.

In order to verify the calculation of the mixed air convection in the post chamber, we measured the fiber temperature

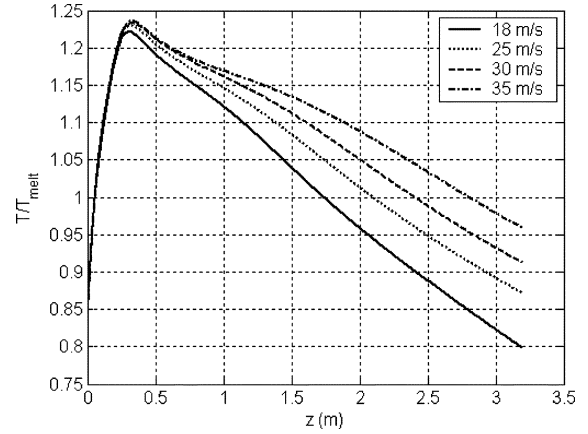


Fig. 7. Glass axial temperature distributions.

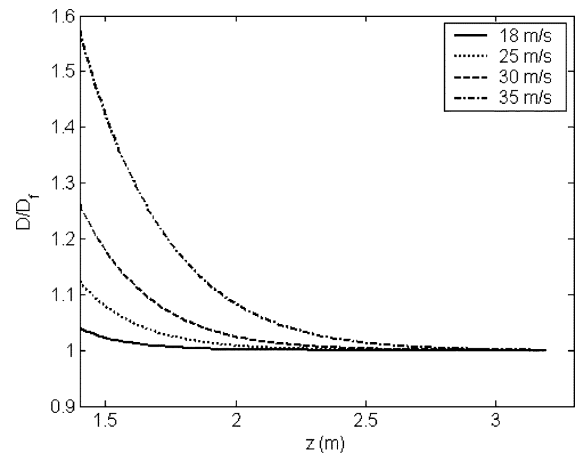


Fig. 8. Glass diameters converging to solidified fibers.

TABLE II  
FIBER SOLIDIFICATION LOCATIONS

$v_f$ (m/s)		18	25	30	35
$L_s$ (m)	Based on $D_f$	1.84	2.20	2.44	2.82
	Based on $T_s$	1.73	2.05	2.32	2.71

at the post-chamber exit using an infrared thermo camera. The measurement (taken on a fiber drawn at 30 m/s) was around 1400 K, which is within 1% of the simulation result of 1418 K. In addition, the temperatures were taken at several locations along the inner wall of the post-chamber using thermocouples for the case of 35-m/s draw speed. Fig. 9 compares the calculated post-chamber wall temperature against the measured data. The close agreement validates the 2-D mixed air convection model for estimating the fiber and the post-chamber wall temperatures.

Other observations are briefly summarized as follows.

- In the post-chamber, the glass cools at a slower rate with higher draw speeds, indicating that advection has a stronger effect than air convection (which increases as the Reynolds number increases with the draw speed) on the glass.
- For all four draw speeds, the glass solidifies well outside the furnace but inside the post-chamber. Models assuming that the glass solidifies within the furnace are not valid. For draw speeds higher than 40 m/s, the fiber may solidify

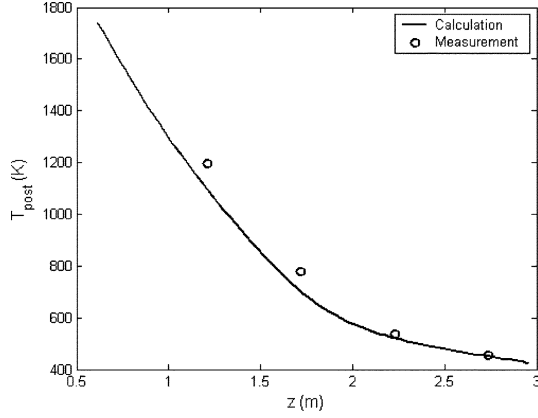
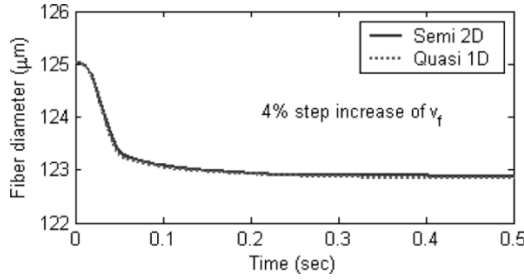
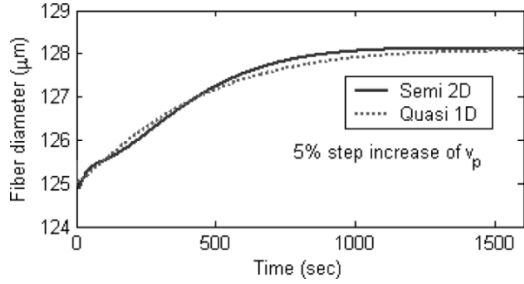


Fig. 9. Post-chamber inner wall temperature.

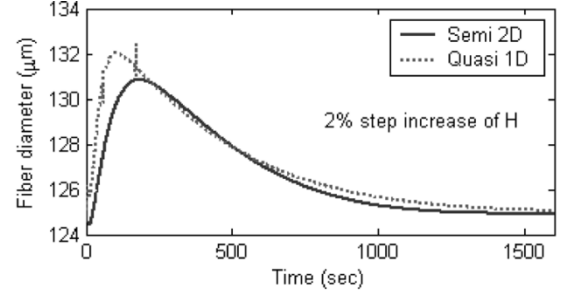
Fig. 10. Step responses to 4% increase in  $v_f$ .Fig. 11. Step responses to 5% increase in  $v_p$ .

outside the post-chamber, in which case a longer post-chamber is needed.

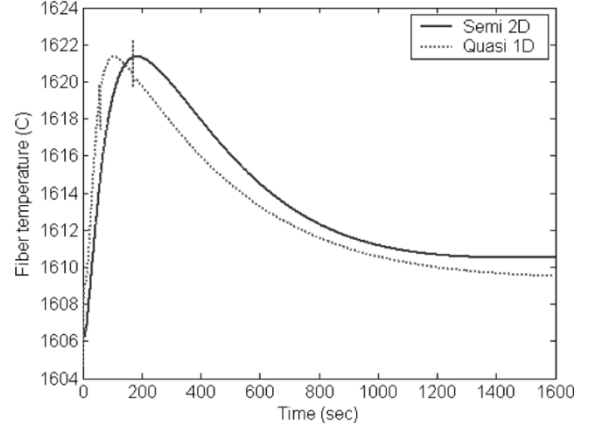
#### D. Transient Responses

Figs. 10, 11, and 12(a) show the simulated responses of the fiber diameters to three different step inputs for TC-II (Table I), where the results are also compared between the semi-2-D and quasi-1-D models. The step magnitudes for the draw speed, preform feedrate, and furnace irradiation were 4%, 5%, and 2% from their respective steady-state values.

As shown in Figs. 10 and 11, the two models agree very well. Some discrepancies in Fig. 12 can be traced to the following reasons. The heat input  $H$  appears explicitly in the energy equation of the quasi-1-D model, but indirectly through the furnace blackbody emissive power  $E_{b,f}$  in the semi-2-D model. To approximately simulate the 2% step change in  $H$ ,  $E_{b,f}$  is increased by 2% in the semi-2-D simulation. Thus, the effective change in  $H$  for the semi-2-D simulation was less than 2% since  $H$  also includes the reflected radiosities originally from the preform, resulting in a slower response and a lower overshoot. As shown in Fig. 12(a), the fiber diameter finally reaches the steady-state value of 125  $\mu\text{m}$  satisfying the continuity of flow. Fig. 12(b)



(a)



(b)

Fig. 12. Step responses to 2% increase in  $H$ . (a) Fiber diameter at the post-chamber exit. (b) Fiber temperature at the post-chamber exit.

shows the fiber temperature response which settles at a higher temperature and the corresponding fiber tension is lower (about 98 g) than the original value.

It is worth noting that the system settling times to a step change in  $v_p$  and  $H$  are in the order of minutes, which are very much slower than that to the draw speed input (in the order of milliseconds). Hence, the effects of high-frequency disturbance (such as the fluctuation in the air convection) can only be attenuated by manipulating the draw speed  $v_f$ .

#### V. CONCLUSION

We have presented computational thermo-fluid models incorporating practically all modes of heat transfer for automating the design of an automated fiber draw process. These models, which relax several assumptions commonly made in modeling draw processes, are applicable to a variety of thermal-fluid systems. Two physical models (semi-2-D and quasi-1-D) are given for a generic furnace/post-chamber system. We have demonstrated how the semi-2-D model can be used to determine the location at which the glass freezes into a fiber, and to provide a detailed description of the 2-D temperature fields and the streamlines to describe the air flow around the converging glass. The location of solidification is important considering that the diameter uniformity must be controlled within 1  $\mu\text{m}$  for a 125- $\mu\text{m}$ -diameter optical fiber, for which the design of a post-chamber becomes essential to gradually cool the fiber in order to reduce optical losses in the final product. The semi-2-D solution also serves a basis for deriving the distributed quasi-1-D model, which explicitly solves for the controlled variables; namely, glass geometry, velocity, and temperature. Despite the emphasis here on

faster draw of glass which is a participating media in radiation, we expect that the extension of the modeling techniques to other processes involving nonparticipating media such as composite, polymer, or synthetic fibers is relatively straightforward.

Both the semi-2-D and quasi-1-D models have been experimentally validated by comparing the computed steady solutions against an experimentally measured neck-down profile of a 9-cm-diameter preform drawn at a high draw speed of 25 m/s, and temperatures taken at strategic locations in the post-chamber wall. Transient responses to three different step inputs were simulated and compared between the two models, which show excellent agreement. We believed that these benchmark data will be useful bases for comparing thermal-fluid models in the future. Finally, we have applied the semi-2-D models to the design of commercial draw towers, which have resulted in a significant reduction of the overall setup time in the production of optical fibers. In addition, we have extended the distributed quasi-1-D model to model-based control system design and implementation to maintain uniformity of fiber diameters [25].

## REFERENCES

- [1] Z. Wei, K. M. Lee, Z. Zhou, and S.-P. Hong, "Effects of radiative transfer modeling on transient temperature distribution in semitransparent glass rod," *ASME J. Heat Transf.*, vol. 125, pp. 1–7, 2003.
- [2] M. A. Matovich and J. R. A. Pearson, "Spinning a molten threadline," *Ind. Eng. Chem. Fund.*, vol. 8, no. 3, pp. 512–520, 1969.
- [3] G. J. Donnelly and C. B. Weinberger, "Stability of isothermal fiber spinning of a Newtonian fluid," *Ind. Eng. Chem. Fund.*, vol. 14, no. 4, pp. 334–337, 1975.
- [4] W. W. Schultz, A. F. Zebib, S. H. Davis, and Y. Lee, "Nonlinear stability of Newtonian fibers," *J. Fl. Mech.*, vol. 149, pp. 455–475, 1984.
- [5] A. Mulpur and C. Thompson, "Nonlinear control of optical fiber diameter variations," *IEEE Trans. Contr. Syst. Technol.*, vol. 4, no. 2, pp. 152–162, Mar. 1996.
- [6] J. R. A. Pearson, Y. T. Shah, and R. D. Mhaskar, "On the stability of fiber spinning of freezing fluids," *Ind. Eng. Chem. Fund.*, vol. 15, pp. 31–37, 1976.
- [7] R. D. Mhaskar and Y. T. Shah, "Stability analysis of glass fiber spinning," *Glass Technol.*, vol. 18, pp. 152–158, 1977.
- [8] F. T. Geyling and G. M. Homsy, "Extensional instabilities of the glass fiber drawing process," *Glass Technol.*, vol. 21, no. 2, pp. 95–102, 1980.
- [9] U. C. Paek and R. B. Runk, "Physical behavior of the neck-down region during furnace drawing of silica fibers," *J. Appl. Phys.*, vol. 49, pp. 4417–4422, 1978.
- [10] G. M. Homsy and K. Walker, "Heat transfer in laser drawing of optical fibers," *Glass Technol.*, vol. 20, no. 1, pp. 20–26, 1979.
- [11] M. R. Myers, "A model for unsteady analysis of preform drawing," *AIChE J.*, vol. 35, no. 4, pp. 592–602, 1989.
- [12] V. N. Vasiljev, G. N. Dulnev, and V. D. Naumchic, "The flow of a highly viscous liquid with a free surface," *Glass Technol.*, vol. 30, no. 2, pp. 83–90, 1989.
- [13] Z. Xiao and D. A. Kaminski, "Flow, heat transfer, and free surface shape during the optical fiber drawing process," in *Proc. ASME National Heat Transfer Conf.*, vol. 9, 1997, pp. 219–229.
- [14] S. R. Choudhury, Y. Jaluria, and H.-K. Lee, "A computational method for generating the free-surface neck-down profile for glass flow in optical fiber drawing," *Num. Heat Transf. A*, vol. 35, pp. 1–24, 1999.
- [15] Z. Yin and Y. Jaluria, "Neck down and thermally induced defects in high-speed optical fiber drawing," *J. Heat Transfer*, vol. 122, pp. 351–362, 2000.
- [16] X. Cheng and Y. Jaluria, "Effect of draw furnace geometry on high-speed optical fiber manufacturing," *Num. Heat Transf.*, pt. A, vol. 41, pp. 757–781, 2002.
- [17] Z. Y. Wei, K.-M. Lee, S. Tchikanda, Z. Zhou, and S.-P. Hong, "Free surface flow in high speed fiber drawing with large-diameter glass preforms," *ASME J. Heat Transf.*, vol. 126, no. 5, pp. 713–722, 2004.
- [18] J. Liu, H. M. Shang, and Y. S. Chen, "Prediction of radiative transfer in general body-fitted coordinates," *Num. Heat Transf. B*, vol. 31, pp. 423–439, 1997.
- [19] S. Banerjee, J. V. Cole, and K. F. Jensen, "Nonlinear model reduction of rapid thermal processing systems," *IEEE Trans. Semiconduct. Manufact.*, vol. 11, no. 2, pp. 266–275, May 1998.
- [20] N. P. Bansal and R. H. Doremus, *Handbook of Glass Properties*. New York: Academic, 1986.
- [21] H. Schlichting and K. Gersten, *Boundary Layer Theory*, 8 ed. New York: Springer-Verlag, 2000.
- [22] M. F. Modest, *Radiative Heat Transfer*. New York: McGraw-Hill, 1993.
- [23] R. I. Issa, "Solution of the implicitly discretized fluid flow equations by operator-splitting," *J. Comput. Phys.*, vol. 62, pp. 40–65, 1985.
- [24] J. Tannehill, D. Anderson, and R. Pletcher, *Computational Fluid Mechanics and Heat Transfer*, 2 ed. New York: Taylor & Francis, 1997.
- [25] K.-M. Lee, Z. Wei, and Z. Zhou, "Modeling by numerical reduction of modes for multi-variable control of an optical fiber draw process," *IEEE Trans. Autom. Sci. Eng.*, vol. 3, no. 1, pp. 119–130, Jan. 2006.
- [26] J. D. Fleming, "Fused Silica Manual," Final Rep. U.S. Atomic Energy Commission, Project no. B-153, Oak Ridge, TN, 1964.

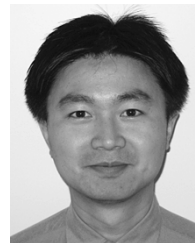


**Kok-Meng Lee** (M'89–SM'02–F'05) received the B.S. degree from the State University of New York, Buffalo, in 1980, and the S.M. and Ph.D. degrees from the Massachusetts Institute of Technology, Cambridge, in 1982 and 1985, respectively.

Currently, he is a Professor in the Woodruff School of Mechanical Engineering at the Georgia Institute of Technology, Atlanta. His research interests include system dynamics/control, robotics, automation, and mechatronics. He holds eight patents in machine vision, three degrees of freedom (DOF) spherical

motor/encoder, and live-bird handling system.

Dr. Lee is a Fellow of ASME. He received the National Science Foundation (NSF) Presidential Young Investigator, Sigma Xi Junior Faculty Research, International Hall of Fame New Technology, and Kayamori Best Paper awards.



**Zhiyong Wei** received the B.S. and S.M. degrees in mechanical engineering from the Shanghai Jiao Tong University, Shanghai, China, in 1996 and 1999, respectively, and the Ph.D. degree in mechanical engineering from the Georgia Institute of Technology, Atlanta, in 2004.

Currently, he is a Computational Fluid Dynamics (CFD) engineer with Caterpillar, Inc., Mossville, IL, working on the development of new diesel engine components. His research interests are on computational modeling and control of dynamic thermal-fluid systems.



**Zhi Zhou** received the M.S. and B.S. degrees in electrical engineering from Jilin University of Technologies, ChangChun, China, in 1986 and 1983, respectively, and the Ph.D. degree in mechanical engineering from the Georgia Institute of Technology, Atlanta, in 1995.

Currently, he is a Manager for the Center of Excellence for Controls at Plug Power, Inc., Latham, NY. Previously, he was a Distinguished Member and Technical Manager with Bell Laboratories of Lucent Technologies, formerly AT&T, Atlanta, GA, where

he was responsible for the optical-fiber draw technology research and development. His research interests include dynamic systems/controls, mechatronics, and fuel-cell systems. He holds nine U.S. patents.



**Siu-Ping Hong** received the B.S. degree in physics from the Chinese University of Hong Kong, Hong Kong, China, in 1970, and the M.S. and Ph.D. degrees in physics from the University of Delaware, Newark, in 1972 and 1975, respectively.

He has been a Member with Bell Laboratories since 1978. As a Distinguished Member in 1984 and Technical Manager in 1990, he has worked on the development of semiconductor circuit assembly and optical-fiber fabrication technologies for 23 years.